Journal of Macromolecular Science, Part A
Publication details, including instructions for authors and subscription information:
http://www.informaworld.com/smpp/title~content=t713597274

Morphological Investigation of Polytetba-Methyleneoxide-Dibbomoxylene Segmented Ionene Polymebs by Tbansmission Electbon Micboscopy and Small-Angle X-Ray Scattebing

Daan Feng[a]; Garth L. Wilkes[a]; Charles M. Leir[b]; John E. Stark[b]
[a] Department of Chemical, Engineering and Polymer Materials and Interfaces Laboratory Virginia Polytechnic Institute and State University Blacksburg, Virginia [b] Special Chemical Division 3M Corporation, St. Paul, Minnesota

To cite this Article Feng, Daan , Wilkes, Garth L. , Leir, Charles M. and Stark, John E.(1989) 'Morphological Investigation of Polytetba-Methyleneoxide-Dibbomoxylene Segmented Ionene Polymebs by Tbansmission Electbon Micboscopy and Small-Angle X-Ray Scattebing', Journal of Macromolecular Science, Part A, 26: 8, 1151 — 1181
To link to this Article: DOI: 10.1080/00222338908052040
URL: http://dx.doi.org/10.1080/00222338908052040

J. MACROMOL. SCI.—CHEM., A26(8), pp. 1151-1181 (1989)

MORPHOLOGICAL INVESTIGATION OF POLYTETRAMETHYLENEOXIDE-DIBROMOXYLENE SEGMENTED IONENE POLYMERS BY TRANSMISSION ELECTRON MICROSCOPY AND SMALL-ANGLE X-RAY SCATTERING

DAAN FENG and GARTH L. WILKES*

Department of Chemical Engineering and
Polymer Materials and Interfaces Laboratory
Virginia Polytechnic Institute and State University
Blacksburg, Virginia 24061-6496

CHARLES M. LEIR and JOHN E. STARK

Special Chemical Division
3M Corporation, 3M Center
St. Paul, Minnesota

ABSTRACT

A series of segmented ionene polymers with polytetramethyleneoxide (PTMO) soft segments and dibromoxylene hard segments have been studied by small-angle x-ray scattering (SAXS) and by transmission electron microscopy (TEM). As detected by SAXS, these materials display multiple scattering peaks which have not been observed before in ion-containing polymers. For the ionene having the shortest PTMO soft segments, a "rodlike" structure has been observed by TEM, which is in good agreement with the SAXS results. Interestingly, the morphological texture of this material is affected by solution casting even at a very low content of the ionic component (<6.4 vol%). To the author's knowledge, this work represents the first direct observation of domain structure in ionene elastomeric polymers. Based on these data, a tentative morphological model of this ionene system is proposed.

INTRODUCTION

There has been much interest in ion-containing polymers over the last two decades based on numerous publications, books, and proceedings of conferences directed toward this subject matter [1-3]. Always of strong interest has been verification of the multiplet structure or clustering of ion/ion interactions that occurs in these materials by scattering and/or electron microscopy techniques, the latter of which have not been particularly successful. The principal techniques that have displayed the presence of ion clustering are those of small-angle x-ray scattering (SAXS) and small-angle neutron scattering (SANS). There have been numerous models proposed to account for the observed scattering, and controversy still continues as to their validity and application. While these models differ somewhat in their nature, there is general agreement that some form of clustering and/or domain formation occurs in these materials even at relatively low ion contents, i.e., low volume percentages of the ion-containing species.

As alluded to above, two basic types of ion aggregates have been proposed: multiplets and clusters [4, 5]. Multiplets are viewed by Eisenberg to be generally less than eight ion pairs randomly dispersed throughout the polymer matrix. A cluster, however, represents a larger scale of aggregation of multiplets to form a region rich in ionic species with a somewhat depleted zone of the ionic species surrounding them.

The scattering techniques of SAXS and SANS have shed considerable light on the state of the ion clustering, but no completely acceptable model of the structure has been formed. One cause for this lack of acceptance has been the inability of any model to date to account easily for the excessive low-angle scattered intensity typically seen from either SAXS or SANS studies. However, recent studies of Galambos et al. [6] on solution-cast films of sulfonated polystyrene have suggested that the excess low-angle behavior extends from random ion pairs (multiplet) which have not organized into cluster regions. This proposal was based on observing the SAXS behavior of these systems as a function of specific thermal histories. While considerable progress has been made in utilizing scattering methods to decipher the morphological texture of many different types of ionomers, there remains considerable need for further clarification. Furthermore, a single model may not, in fact, suffice for all ionomer system such as random copolymers versus telechelics.

Attempts to image an ionic domain or cluster directly by transmission electron microscopy (TEM) have yielded various results [9-11] depending on the particular ionomers, but again the exact arrangement of the ionic morphology within the nonpolar matrix is still largely unknown. This in-

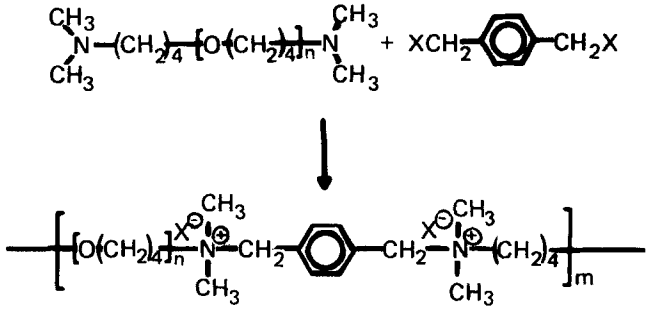

X= Cl, Br, or I

SCHEME 1.

ability of past TEM investigations to verify a specific morphology have been limited by resolution and related focus problems in view of the small dimensional scale of the represented cluster size and their separation distance relative to the film thickness necessary for imaging.

In our recent studies of ionomers, we have begun to investigate the structure-property systems based on ionene chemistry. Ionene polymers, as originally defined by Rembaum et al. [13], are cationic polyelectrolytes with cations based on amines in the backbone. These systems are generally derived from quaternary ammonium salts and can be prepared by a variety of methods [14-16]. The system in which we have been principally interested utilizes a dimethylamino-terminated polytetramethyleneoxide (PTMO) oligomer that is then reacted with 1,4-dibromo-*p*-xylene to directly provide an ionene polymer as illustrated in Scheme 1.

Earlier studies [14, 17] on these ionene polymers showed that these materials display high-strength elastomeric behavior. The results from thermomechanical analysis (TMA), dynamic mechanical analysis (DMA), and small-angle x-ray scattering (SAXS) studies indicate that the good elastomeric mechanical behavior results from a very high degree of phase separation in these materials. The high degree of phase separation is induced by the coulombic or electrostatic interaction of the ionic groups, in contrast to any incompatibility caused by the difference in the solubility parameter characteristics of the two components, PTMO and 1,4-dibromo-*p*-xylene.

Results from SAXS studies also indicate that the morphological structure

or ion clustering in these materials changes with ionic content. The ionic content can be systematically altered by changing the molecular weight of the PTMO elastomeric soft segment. As the ionic content increases, the scattering intensity increases, while a long-range-ordered structure is developed even with a relative low ion content (ca. 6.4 vol%). This long-range-ordered structure and the low ionic concentration make it possible to study the morphological structure of these materials by TEM techniques.

Before discussing our current results obtained from TEM studies of these novel materials, a brief review on the theory of TEM image formation is considered necessary in view of the results to be presented.

Image Formation

Two types of contrast can arise in TEM images: amplitude contrast and phase contrast. Amplitude contrast is due to the elastic scattering of electrons, and it arises from fluctuations in density, atomic number, or thickness of a specimen. Both mass-thickness and diffraction contrast contribute to amplitude contrast. Also, the level of amplitude contrast is strongly dependent on the accelerating voltage and the atomic number of the scattering atoms. This form of contrast can be directly interpreted at medium resolution, which is typically taken to mean specimen detail on a scale greater than 1 nm. In general, amplitude contrast is dominant for large structures while phase contrast is dominant for small structures and becomes the principal or sole source of contrast for very small object points of low atomic number components [31].

Phase contrast, which is produced by interference of the unscattered electron wave and the scattered electron wave, is only slightly dependent on the accelerating voltage and the atomic number of the scattering atoms. An object which does not significantly alter the amplitude of the transmitted electron waves is called a weak-phase object. Most unstained polymer specimens are weak-phase objects. The image of such an object must be interpreted by utilizing transfer theory, which has been developed in detail in many texts [18-20]. A simplified form of transfer theory has been provided by Thomas et al. [11, 21-24] and applied to polymers. The pertinent transfer theory will be briefly reviewed here, for it greatly relates to our results and their interpretation.

The microscope object function, denoted as $\psi(\mathbf{r})$, is directly related to the mean inner potential $\phi(\mathbf{r})$ as

$$\psi(\mathbf{r}) = \frac{\pi}{\lambda V_0} t\bar{\phi}(\mathbf{r}), \tag{1}$$

where λ is the wavelength, V_0 is the accelerating voltage, t is sample thickness, and $\mathbf{r}$ is a position vector between two scattering points. For polymer solids, the mean inner potential may be estimated by [23]

$$\bar{\phi}(\mathbf{r}) = 60 \frac{\rho}{M} \sum n_i f_i, \tag{2}$$

where ρ is the density (g/mL) of the polymer, M is the molecular weight of the repeat unit, f_i is the electron scattering factor at zero angle of the ith type atom, and n_i is the number of the ith type atom in the repeat unit. For a phase-separated segmented polymer in which the two segments are formed by repeat units 1 and 2, the mean inner potential difference between them can be calculated by

$$\Delta\bar{\phi}(\mathbf{r}) = 69\left\{\frac{\rho_1}{M_1}\sum \mathbf{n}_i \mathbf{f}_i^{(1)} - \frac{\rho_2}{M_2}\sum \mathbf{n}_i \mathbf{f}_i^{(2)}\right\}, \tag{3}$$

and the relative phase shift between domains, $\Delta\psi(\mathbf{r})$, is simply

$$\Delta\psi(\mathbf{r}) = \frac{\pi}{\lambda V_0} t\Delta\bar{\phi}(\mathbf{r}). \tag{4}$$

For a weak-phase object, $\psi(\mathbf{r})$ can be described by a phase term: exp $[i\psi_{ph}(\mathbf{r})]$. According to the first Born approximation [18], the object function becomes

$$\psi(\mathbf{r}) = \exp\,[i\psi_{ph}(\mathbf{r})] \simeq 1 + i\psi_{ph}(\mathbf{r}). \tag{5}$$

For the bright-field axial image, the image intensity $\mathbf{I}(\mathbf{r})$ is just the inverse Fourier transform ($\mathbf{F}^{-1}$) of a δ function and a term involving the Fourier transform of the object function, $\mathbf{F}[\psi(\mathbf{r})]$, modulated by the transfer function $T(\mathbf{K})$ of the microscope:

$$\mathbf{I}(\mathbf{r}) = \mathbf{F}^{-1}\left\{\delta(\mathbf{K}) - 2T(\mathbf{K})\mathbf{F}[\psi(\mathbf{r})]\right\}. \tag{6}$$

In Eq. (6), $\mathbf{K}$ is the scattering vector, $|\mathbf{K}| = (4\pi/\lambda)\sin\theta$, and θ is half of the radical scattering angle. The transfer function, $T(\mathbf{K})$, is given by

$$T(\mathbf{K}) = A(\mathbf{K})\sin\,[-\chi(\mathbf{K})], \tag{7}$$

where $A(\mathbf{K})$ is the objective aperture function. The value of $A(\mathbf{K})$ is unity inside the objective aperture and zero outside. The phase shift $\chi(\mathbf{K})$ is given by

$$\chi(\mathbf{K}) = \pi\lambda(\Delta f)\mathbf{K}^2 + \frac{\pi}{2} C_s\lambda^3\mathbf{K}^4, \tag{8}$$

where Δf is the defocus and C_s is the spherical aberration coefficient of the object lens of the microscope. In Eq. (8), the effects of incoherent and chromatic aberrations are neglected. Image contrast is then given by

$$\frac{\mathbf{I}(\mathbf{r}) - \mathbf{I}_{av}}{\mathbf{I}_{av}} = \mathbf{F}^{-1}\left\{2A(\mathbf{K}) \sin \chi(\mathbf{K})\mathbf{F}[\psi(\mathbf{r})]\right\}. \tag{9}$$

Equation (9) indicates that image contrast for a weak-phase object is governed by the Fourier transform of the object function and the transfer function of the microscope. If $\sin \chi(\mathbf{K}) = 1$ for all $\mathbf{K}$, the microscope would be a perfect phase-contrast microscope, and the image contrast would be interpreted intuitively. In practice, the value of $\sin \chi(\mathbf{K})$ is very sensitive to the state of defocus [11, 18-24]. The effects of defocus on $\sin \chi(\mathbf{K})$ for the JEOL 2000EX microscope used in our study, in which the C_s has a value of 1.4 mm, is plotted in Fig. 1. At zero defocus ($\Delta f = 0$), $\chi(\mathbf{K})$ is determined solely by the spherical aberration of the microscope, which is significant only at higher spatial frequencies. For larger scale distances, i.e., $\mathbf{K} < 1.5$ nm^{-1}, $\sin \chi(\mathbf{K})$ is near zero. For the case of the JEOL 2000EX, the calculated optimum defocus value is around -67.4 nm. In this case, $\sin \chi(\mathbf{K})$ is close to -1.0 in the range $1.6 < \mathbf{K} < 3.3$ nm^{-1}. Also in this region, image contrast is identical with the object transform. For a defocus of -202.2 nm, the peak of normal phase contrast is sharpened and moves to lower spatial frequencies. A periodic spacing between 5.0 and 2.5 nm ($0.2 < \mathbf{K} < 0.4$ nm^{-1}) will then be imaged with enhanced phase contrast, and artifacts will occur for resolution beyond 2.0 nm or $\mathbf{K} > 1.0$ nm^{-1}. Because of the sign change of $\sin \chi(\mathbf{K})$ at higher frequencies, a "salt and pepper" phase contrast structure will often be exhibited with the exact texture being dependent on the optical conditions of the microscope employed.

The first-order expression for the image transform, Eq. (9), arises from the interference between the imaginary scattered wave and the unscattered or background wave. Therefore, the image contrast arises from phase contrast, and the image corresponds to the phase-contrast image. However, the modification of the wave in the diffraction plane by the aperture function

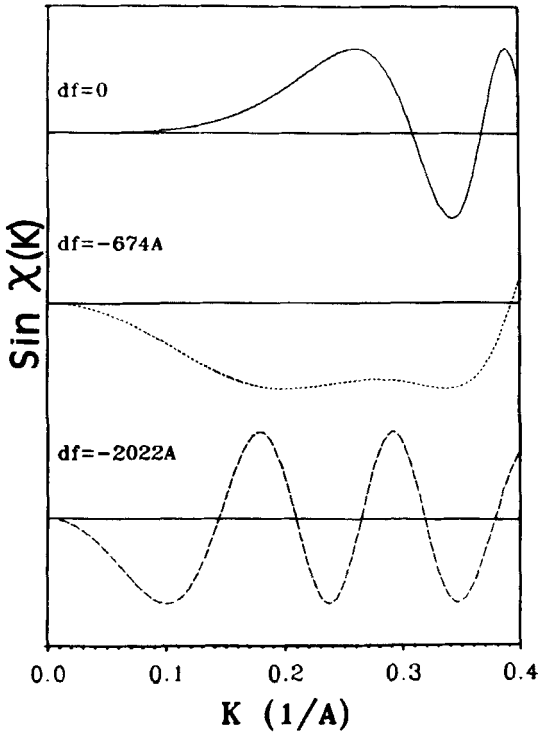

FIG. 1. The effect of defocusing of the transfer function for the JEOL 2000EX microscope. The value of C_s is 1.4 mm, and $\lambda = 0.0025$ nm. Coherent illumination was assumed.

would account for the loss of electrons scattered outside the aperture, and the effects of amplitude contrast should arise naturally.

To describe the effects of amplitude contrast, an extra amplitude term $\exp[\psi_{ampl}(\mathbf{r})]$ is introduced into Eq. (5), and $\psi(\mathbf{r})$ becomes

$$\psi(\mathbf{r}) = \exp[\psi_{ampl}(\mathbf{r})] \exp[i\psi_{ph}(\mathbf{r})]. \tag{10}$$

By employing the first-order approximation, the object function is estimated by

$$\psi(\mathbf{r}) \simeq 1 + \psi_{ampl}(\mathbf{r}) + i\psi_{ph}(\mathbf{r}). \tag{11}$$

In this case both the ψ_{ph} and ψ_{ampl} terms must be smaller than unity for the first-order approximation. The image contrast then becomes

$$\frac{\mathbf{I(r)} - \mathbf{I}_{av}}{\mathbf{I}_{av}} = \mathbf{F}^{-1}\left\{\mathbf{F}[\psi(\mathbf{r})]\, 2A(\mathbf{K})[\sin\chi(\mathbf{K}) + Q(\mathbf{K})\cos\chi(\mathbf{K})]\right\}. \tag{12}$$

In Eq. (12) the maximum possible contribution from amplitude contrast relative to that from phase contrast is given by the factor $Q(\mathbf{K})$, having the form of

$$Q(\mathbf{K}) = \frac{S_t A}{2\lambda N \mathbf{f}}, \tag{13}$$

where $\mathbf{f}$ is the electron scattering factor, S_t is the total cross section per gram of matter for scattering outside a given object aperture, A is the atomic number, and N is Avogadro's number. Experimental results of Burge and Smith [25] have given the value of $S_t = 1.2 \times 10^5$ cm^2/g, which was correct for all elements at 75 kV. By employing this estimated S_t value, $Q(\mathbf{K})$ is estimated as 0.12 for carbon, 0.26 for bromine, and 0.4 for uranium at 75 kV. These values may be lower if a larger aperture or higher accelerating voltage is used. Because of the theoretical uncertainties, the most direct approach to determining $Q(\mathbf{K})$ is to obtain it experimentally. Experimental results [26] indicate that the $Q(\mathbf{K})$ is about 0.4 at $\mathbf{K}$ less than 0.2 nm^{-1}, and it decreases to less than 0.1 for $\mathbf{K} > 0.5$ nm^{-1} for uranium. These results are consistent with the value predicted above, but show that amplitude contrast is most important at low resolution.

By employing a value of 0.4 for $Q(\mathbf{K})$ into Eq. (12), the function $[\sin\chi(\mathbf{K}) + Q(\mathbf{K})\cos\chi(\mathbf{K})]$ vs $\mathbf{K}$ is shown in Fig. 2. At zero defocusing, the results indicate that for $\mathbf{K} < 1.0$ nm^{-1} there is no sign change. In other words, the image contrast obtained for $\mathbf{K} < 10$ nm^{-1} arises from amplitude contrast.

In the case of our PTMO ionene polymer, the *difference* in the inner potential $\phi(\mathbf{r})$ of the two components, PTMO and dibromoxylene, is about 2.23 V, as extimated by Eq. (3) with zero angle scattering factor [27], which is quite high (e.g., compare this with the value of 1.65 V for a segmented polyurethane with hard segments of 4,4'-diphenylmethane diisocyanate (MDI) and 1,4 butenediol and with soft segments of MDI and poly(propylene oxide)diol [22]). If we limit the phase shift $\Delta\psi(\mathbf{r})$ to less than 0.5 radian for a weak-phase object, the thickness of the ionene specimen which one could wish to investigate should be less than 30 nm as estimated by Eq. (4). In practice, the cryomicrotomed sections we have utilized in this work have a thickness of

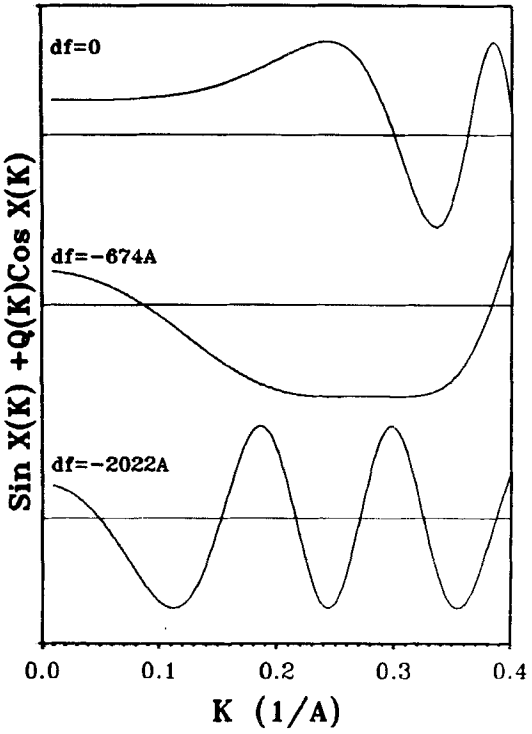

FIG. 2. The effect of the mass-thickness contrast on the transfer function for the JEOL 2000EX. The value used is for $Q(\mathbf{K}) = 0.4$.

the order of 50 nm. Therefore, mass-thickness contrast should also contribute to the final image.

Besides the thickness effects, the geometry of the domain structure is also a key factor. The TEM image is a two-dimensional projection of the three-dimensional specimen. Scheme 2 shows just three possible geometries of domain structures. If the domain thickness and the film thickness are similar (Scheme 2a) or the domain thickness is much smaller than the film thickness but a long-range-ordered structure is presented (Scheme 2b), the projected image is uncomplicated, and correct interpretation of the domain image is possible. In the latter case, Scheme 2b, the diffraction contrast will also contribute to the image contrast. However, if the domain size is smaller than the film thickness and the domains are randomly distributed, the resulting projection will be almost in-

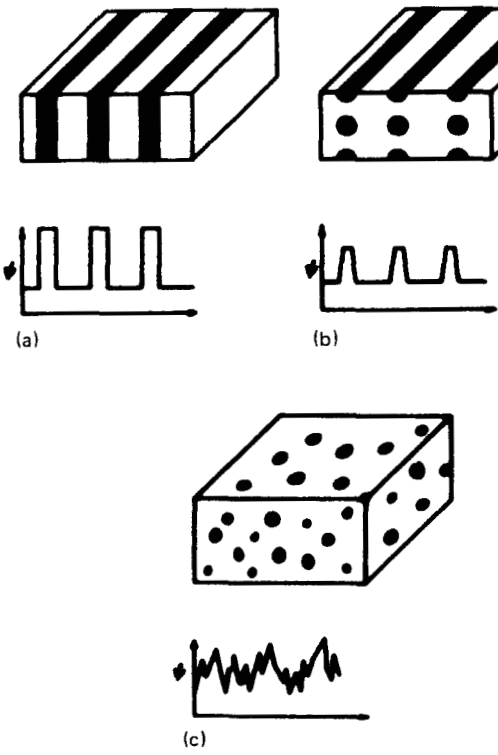

SCHEME 2.

distinguishable from random noise (Scheme 2c). In this case a very thin specimen must be prepared to resolve this problem. In general, the thickness of a cryomicrotomed section is on the order of a few hundred Angstroms to 100 nm. The domain or cluster structure of ionomers studied by others is believed generally to have a "spacing" or correlation length under 10 nm, as determined by SAXS. Therefore, it is quite understandable that the previous TEM studies have produced a wide variation of the postulated "domain types" and "size," while the SAXS results were similar [8-11]. With this material as background for our TEM studies, we will proceed to the details of our investigation and the corresponding results.

EXPERIMENTAL

Materials

Preparation of the segmented PTMO-ionene polymers has been described elsewhere [15]. The ionenes studied are designated as

IB-NS-18

- IB-NS-18
  - PTMO segment molecular weight/100
  - architecture of the coupling agent.
    - NS = 1,4-dibromo-*p*-xylene
  - type of counterion. B = bromide.

Films of these ionenes were prepared by solution casting from chloroform at ambient temperature on a Teflon surface over a period of 2-3 days. The films were dried at 80°C in vacuo for 24 h after casting. The films were stored in a vacuum desiccator until used. Some compositional features of these ionenes are listed in Table 1.

Techniques

Small-Angle X-Ray Scattering (SAXS)

An automated Kratky-slit collimated camera equipped with a M. Braun position-sensitive detector was utilized for the intensity measurements of small-

TABLE 1. Composition of PTMO Ionenes

Sample	PTMO block, $\bar{M}_n$	% Ionic concentration[a]	Hard segment, vol%
IB-NS-18	1800	8.0	6.6
IB-NS-26	2600	5.6	4.7
IB-NS-34	3400	4.3	3.6
IB-NS-66	6600	2.2	1.0

[a]Per PTMO repeat unit.

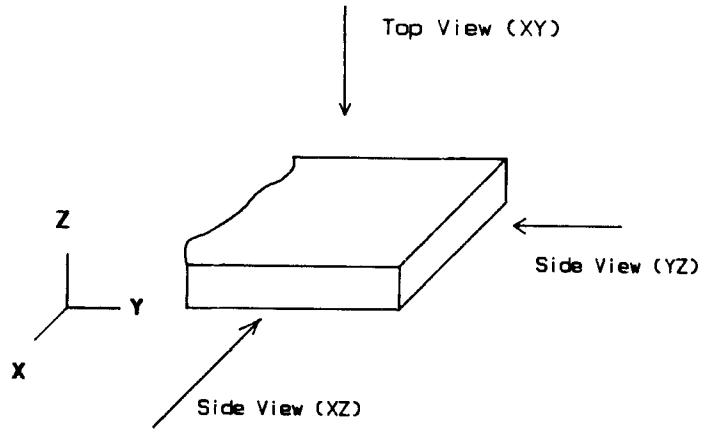

SCHEME 3.

angle scattering. In all of these tests the incident x-ray beam was parallel to the normal of the surface of the solution-cast film (see Scheme 3). In addition, a simple Warhus camera with pinhole collimation utilizing a flat plate film cassette was also used. With this device the beam was passed either parallel or perpendicular to the normal of the film surface with an appropriate exposure time to provide direct recording of the intensity under vacuum. All SAXS measurements presented in this paper were obtained at ambient temperature.

Transmission Electron Microscopy (TEM)

A JEOL 2000EX transmission electron microscope (TEM) was operated at 200 kV for all the TEM experiments with optimum adjustment of astigmatism. Ultrathin sections of the ionene films were microtomed at -100°C with a Reichert-Jung ULTRAVUTE System FC4. The ultrathin sections were cut in three different directions (Scheme 3); one parallel to the film surface (*xy*-plane) and the others perpendicular to it (*xy* and *yz* planes). High contrast was obtained due to the high electron density of the moieties containing ionene halide compared to the PTMO soft segments.

RESULTS AND DISCUSSION

The general characteristics of solution-cast ionene films are that they display high-strength elastomeric behavior with good extensibility and recoverability [17]. At high strain, induced crystallization of the PTMO segments occurs in all samples. However, the undeformed samples have no sign of PTMO crystallization at room temperature for PTMO segment molecular weights less than 3400. For the samples containing higher molecular weight PTMO segments, IB-NS-34 and IB-NS-66, the crystallization at room temperature does occur at a slow rate (over a week) to develop a detectable amount of crystallinity, but these samples will not be discussed in detail in this paper. In order to eliminate any possible effects of the PTMO crystallinity on the SAXS pattern, all samples were heated at 60°C for 2 h prior to SAXS studies to remove any possible traces of srystallinity of the PTMO segments.

Earlier studies [17] indicate that the distinct elastomeric behavior of these materials is an indication of a very high degree of microphase separation. Figure 3 shows the SAXS intensity profiles of the ionenes obtained from the Kratky camera. As noted, there are very distinct maxima in the SAXS profiles. In this figure the angle-dependent variable is expressed as s ($s = (2/\lambda) \sin \theta$, and θ equals 1/2 of the radical scattering angle). The SAXS results of the ionene with the longest PTMO segments, IB-NS-66, is rather similar to the SAXS profile of a telechelic ionomer which has been investigated in this laboratory and discussed elsewhere [28]. In fact, the basic single shoulder in the SAXS profile is quite typical of most ionomers samples studied by other laboratories [11, 12]. For the case of our segmented ionene systems, the high scattered intensity near zero angle may arise from randomly placed ionene linkages, and the stronger single peak intensity may similarly result from the scattering from ion clusters or domains [12]. For our materials the peak "Bragg" or correlation distance in our case may be interpreted as the interdomain or intercluster distance. This estimated Bragg distance and the scattered intensity of the ionenes are both strongly dependent upon the PTMO segment length as shown in Fig. 3 and Table 2. One sees that the first peak spacing decreases as the PTMO segment length decreases. This, of course, suggests that the spacing is directly related to an average interparticle or interdomain spacing between the ionene-containing domains and is in line with earlier observations of Teyssié et al., although their materials were telechelic in nature (not segmental) and they were not based on ionene chemistry [29].

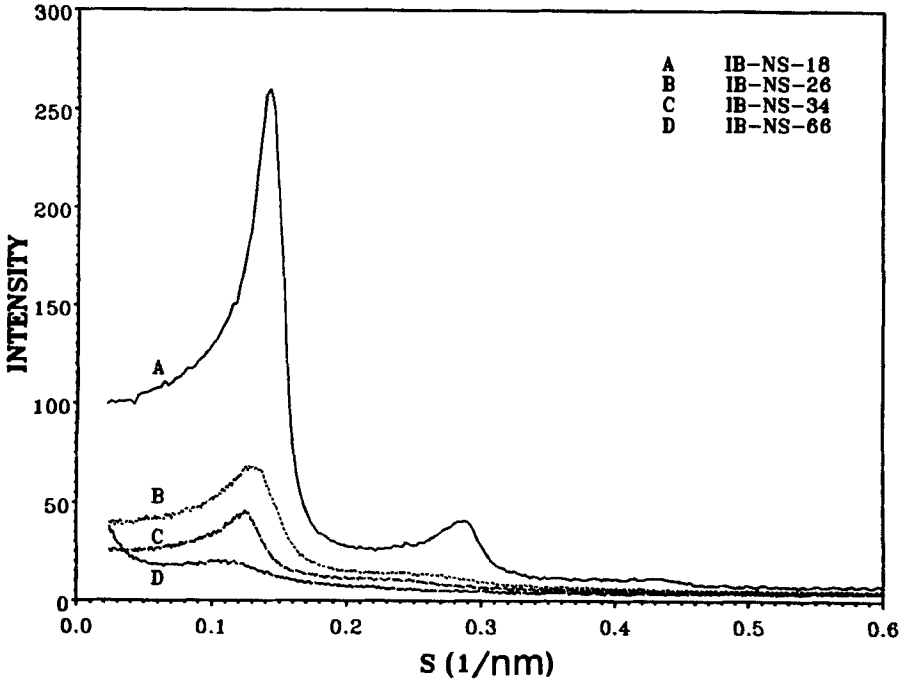

FIG. 3. Smeared SAXS profiles of some of IB-NS ionene polymers obtained with the Kratky camera.

The peak intensity of ionenes (particularly those of higher ionene content) is high, and the peaks of the ionenes are also much more distinct than usually noted for ionomers or, in fact, for related segmented polymers that developed domain structure by segment incompatibility, e.g., the segmented urethanes [33]. While the high intensity and the sharpness might also relate to the narrow molecular weight distribution of the PTMO segments, we strongly believe that it is from induced long-range order structure, as discussed below.

Another and more noteworthy feature of our ionenes consists of the *multiple* scattering peaks. The effect of the PTMO segment length on the morphological structure of the ionenes is also shown in Fig. 3. As the PTMO segment length decreases or increases in ion content (Table 1), the peak intensity increases and a second scattering peak develops. Also, a distinct downturn at low s is observed compared to the intensity of the first maximum. For sample

IB-NS-18, which contains the shortest PTMO segments, a very weak third peak is observed even from the smeared SAXS profile (Fig. 3, Curve A). It is noteworthy that this observation of three scattering peaks has never been observed in a segmented ionene material, let alone any other ionomer materials, as far as we are aware. The estimated Bragg spacing calculated from the smeared SAXS profile of IB-NS-18 shows a relationship close to 1:2:3 for the first three peaks, with the first order being 7.0 nm. (There is a small question of whether the multiple SAXS peaks arise from increasing orders of scattering, as will be discussed later.) This general scattering behavior suggests a lamellar structure with considerable long-range order similar to the scattering behavior that has been observed in certain of styrene-isoprene and related block polymers [34]. Such a morphological structure is somewhat surprising because the content of hard segment is only ~6 vol% for the IB-NS-18 polymer.

By utilizing the unsmeared pinhole collimation of a Warhus camera, the two-dimensional scattering pattern for the IB-NS-18 ionene was also obtained and is shown in Fig. 4 (with the beam parallel to the film normal). The result is in very good agreement with the earlier results from the slit-collimated experiments. In fact, even a fourth maximum is observed with long exposure time. The spacings from the multiple rings scale again are nearly 1:2:3:4, with the first being ~6.5 nm, which is consistent with the largest spacing calculated from the desmeared data from the Kratky camera [30]. As an important reminder, the SAXS results in both Figs. 3 and 4 were obtained by passing the x-ray beam normal to the film surface (see Scheme 3).

As stated above, the high scattering intensity of these ionenes is undoubtedly caused by good phase separation of the units containing high-electron-dense ionene from that of the relatively low electron density PTMO segments. The Porod analysis (which will be provided in a later paper) of the high angular scattering intensity (the tail region of the SAXS profile) indicates that the thickness of domain interface is in order of 0.1-0.2 nm which is quite small, providing another good indication of a very high degree of phase separation.

The extremely high degree of phase separation, long-range order, and small hard-segment volume fraction of these materials, especially for IB-NS-18, tempted us to investigate ultrathin cryomicrotomed sections from the same solvent cast films by transmission electron microscopy (TEM). In order to study the spatial microstructure of this material, the ultrathin sectioning was carried out such that the morphological features could be investigated for all three observation directions (see Scheme 3).

The TEM studies were carried out on a JEOL 2000EX microscope. The astigmatism of the microscope was well adjusted. A 200-kV accelerating

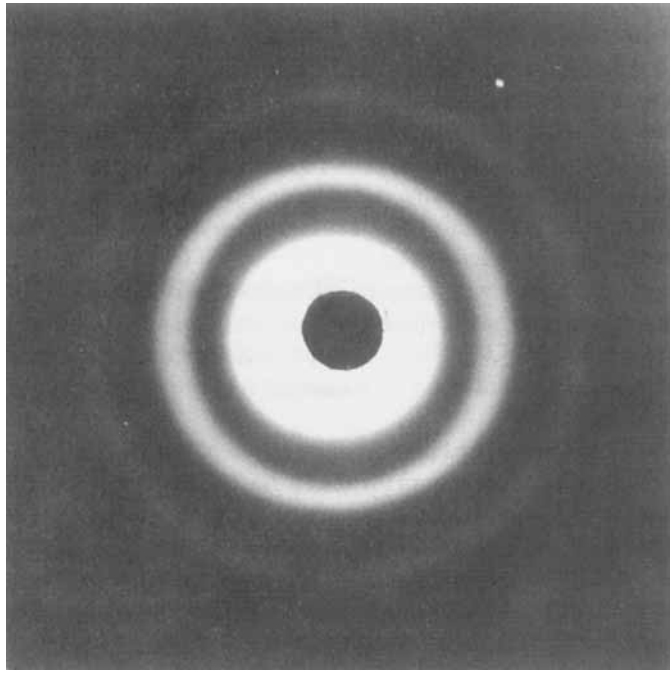

FIG. 4. SAXS pattern of IB-NS-18 obtained from the Warhus camera. The x-ray beam was parallel to the normal of the film.

voltage was used. The high voltage provides higher penetration power while reducing the radiation damage to the sample. Also, the higher accelerating voltage improves resolution due to a shorter wavelength as well as minimizes multiple scattering [31]. The TEM results showed that when a specimen was exposed to the electron beam over 5 min, there was no difference in the texture of the specimen. This implied that there is no significant radiation damage to these samples. A small objective aperture (20 μm) was also used to minimize the artifacts of the microscope at higher spatial frequencies or smaller scale distances.

Figure 5 shows the results of the TEM studies on a IB-NS-18 ionene film. The micrographs were taken at medium resolution (50 000X) and near focus. The dark regions in the micrographs contain the ionene units having the high-electron-density bromide ions. The brighter regions represent the PTMO-

containing regions. Figure 5(a) illustrates the view normal to the surface of the film (*xy* plane in Scheme 3), which displays some phase-separated structure; however, no distinct sheetlike or lamellar or even rodlike structure is observed. In fact, this view is of the rather common "salt-and-pepper" type texture and, thereby, makes one initially cautious with regard to the interpretation of this micrograph. However, the micrographs in Figs. 5(b) and 5(c) present the two "side views" of the same film (*xz* and *yz* planes in Scheme 3), and each shows a very distinct lamellar or rodlike structure with long range order. The periodic spacing of this structure is ~70 Å, which is in direct agreement with the SAXS data. Of particular importance is the fact that this structure is preferentially oriented perpendicular to the surface of the film, apparently as a result of the solution-casting procedure.

This striking morphological structure was verified by defocusing procedures. Figure 6 shows the defocusing pictures as viewed for the *xz* plane. As the focus was varied over the wide range from +67.4 to -1011 nm, the image remains almost unchanged (Fig. 6). These through-focusing pictures indicate that the image obtained mainly results from mass-thickness contrast rather than phase contrast. As mentioned in the earlier sections on transfer theory, phase contrast mostly contributes to the high-spatial-frequency or small-spacing region. Our calculation indicates that artifacts having a spacing of 7.0 nm could be introduced at a defocusing of -10 000 nm. Such a large defocusing is unrealistic in our case. At near focus the value of $\sin \chi(\mathbf{r})$ is almost zero for $\mathbf{K} < 0.1\ \mathrm{nm}^{-1}$, or a physical spacing > 1.0 nm. Therefore, artifacts or an anomalous texture of this type should not be produced for images having a spacing greater than 1.0 nm.

Since the medium-resolution bright-field images exhibit dominantly amplitude contrast under operating near focus [32], the rodlike structure in Figs. 5(b) and 5(c) is believed to arise from amplitude contrast. As Fig. 2 shows, the function $\sin \chi(\mathbf{r}) + Q(\mathbf{r}) \cos \chi(\mathbf{r})$ is about 0.4 in the region of $\mathbf{K} < 0.1\ \mathrm{nm}^{-1}$ or spacing > 1.0 nm and there is no sign change. Therefore, the image in this region arises principally from amplitude contrast. In other words, the image in Figs. 5(b) and 5(c) should represent the real morphological structure of the ionene mentioned.

Further proof of the structure was obtained by passing the x-ray beam through both surfaces and the sides of the film in the Warhus pinhole collimated camera (see Scheme 3). When the beam is parallel to the film normal, the x-ray pattern shows no orientation effects (Fig. 7a). But when the beam is orthogonal to the film normal, the SAXS patterns of Figs. 7(b) and 7(c) were obtained. These patterns clearly and conclusively verify the basic results of the TEM studies. That is there appears to be at least three orders

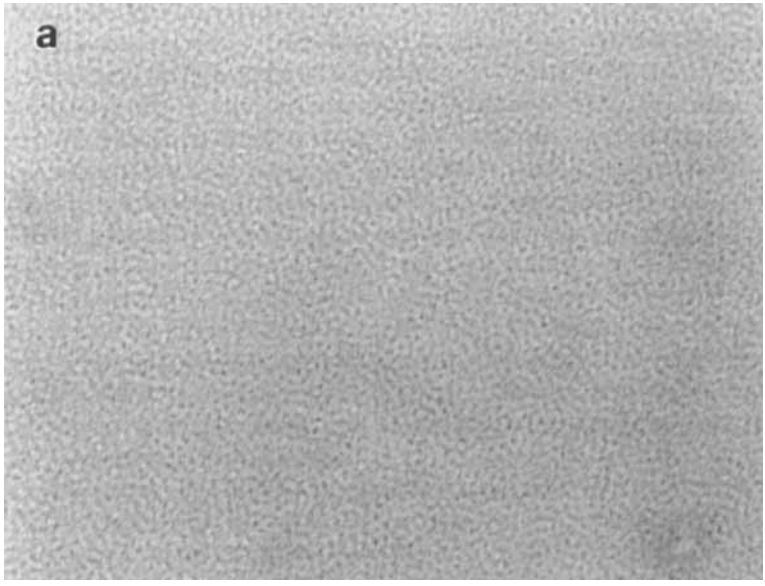

FIG. 5. TEM micrographs of the IB-NS-18 ionene polymer. (a) The top view (xy-plane in Scheme 3). (b) The side view (xz-plane in Scheme 3). (c) The side view (yz-plane in Scheme 3).

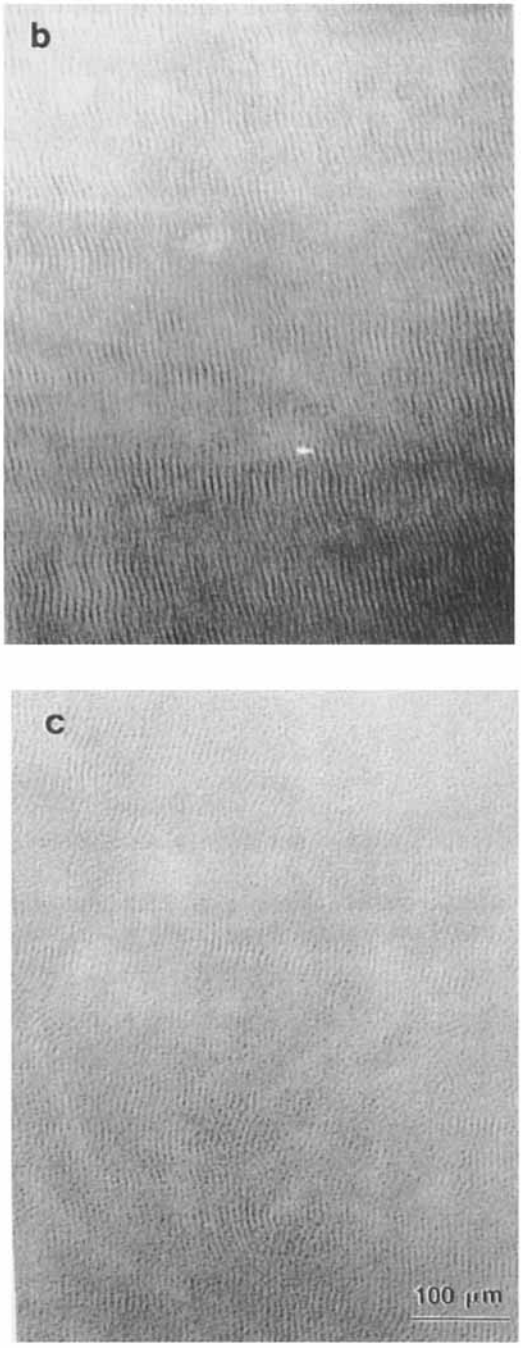

Fig 5(b) and 5(c)

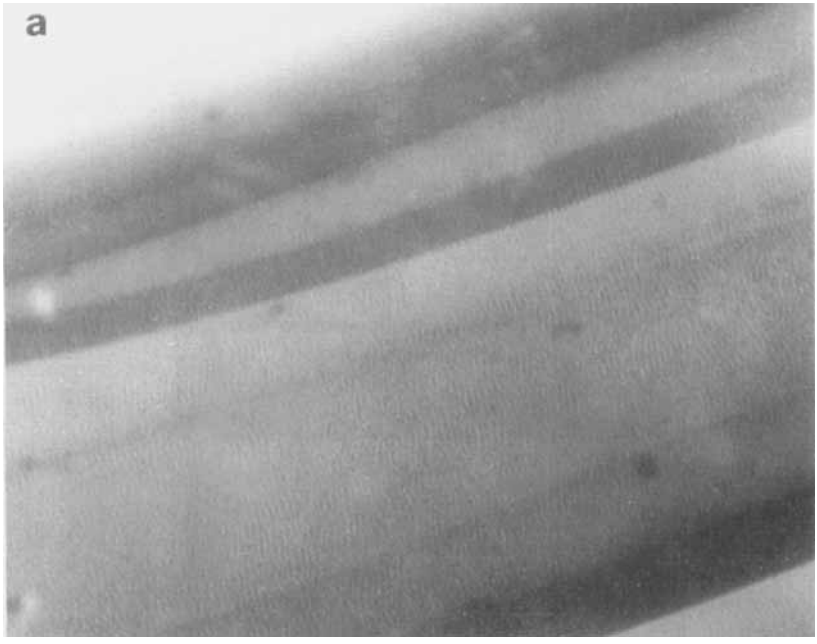

FIG. 6. Side view (*xz* plane) defocusing, *df*, TEM micrographs of Sample IB-NS-18. (a) $df = 67.4$ nm. (b) $df = 0$ nm. (c) $df = -1011$ nm.

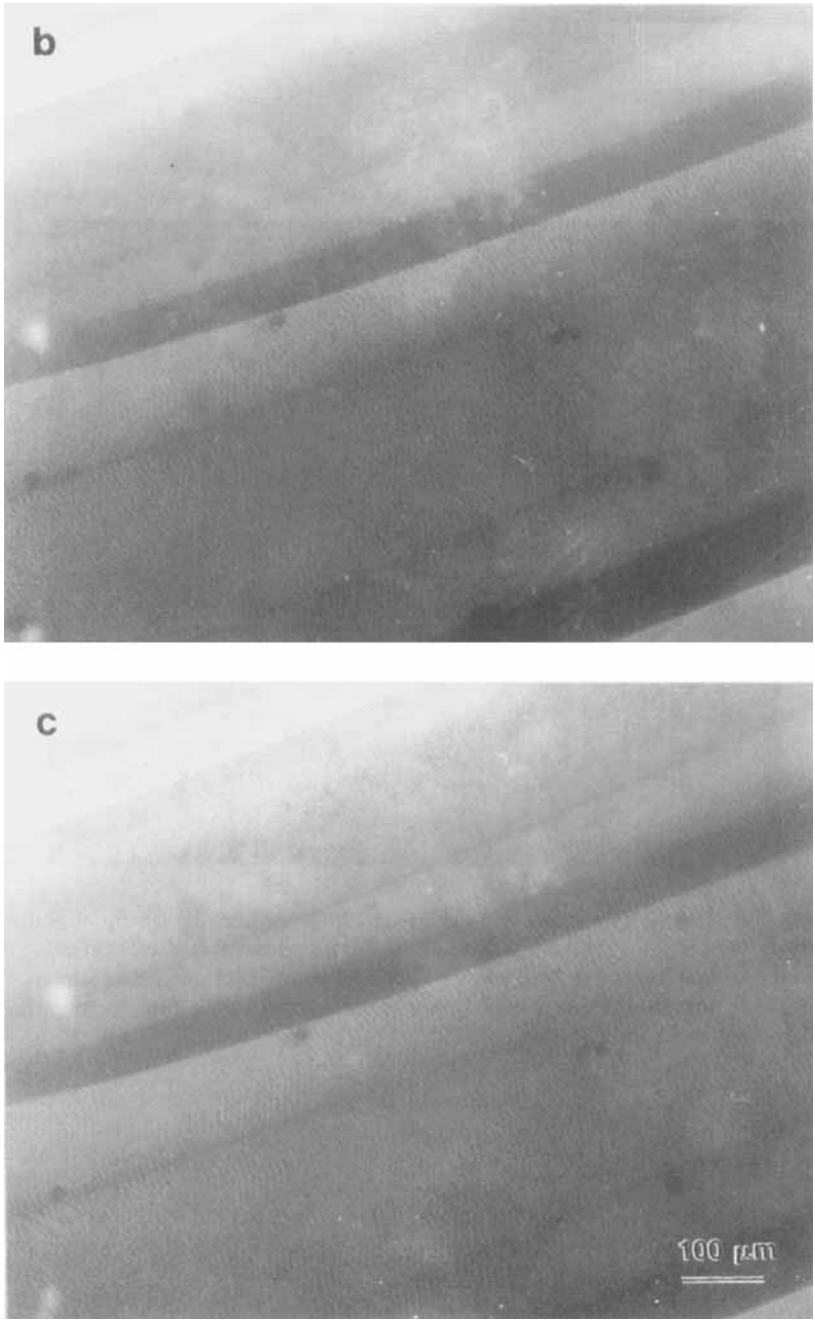

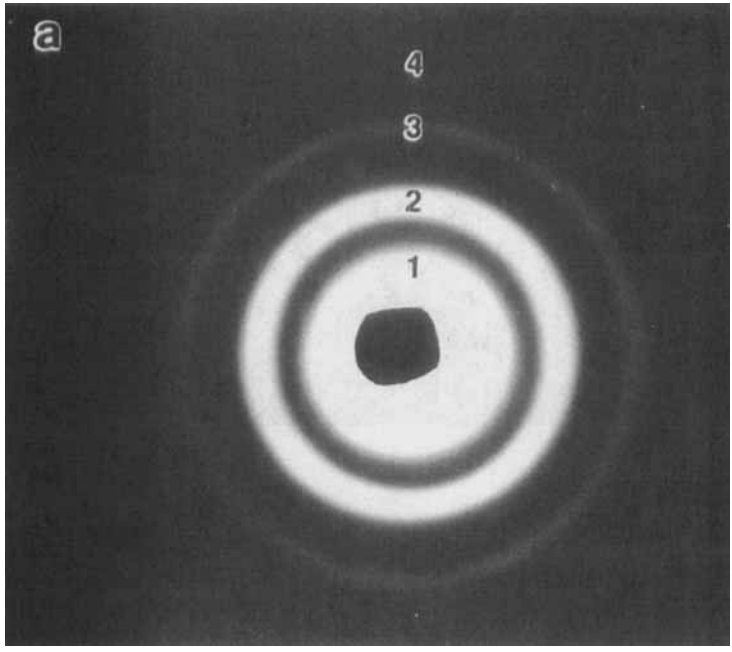

FIG. 7. The SAXS patterns of Sample IB-NS-18 obtained with the Warhus camera. (a) the x-ray beam was parallel to the film normal (z-direction in Scheme 3). (b) The x-ray beam was orthogonal to the film normal (x direction in Scheme 3). (c) The x-ray beam was orthogonal to the film normal (y-direction in Scheme 3).

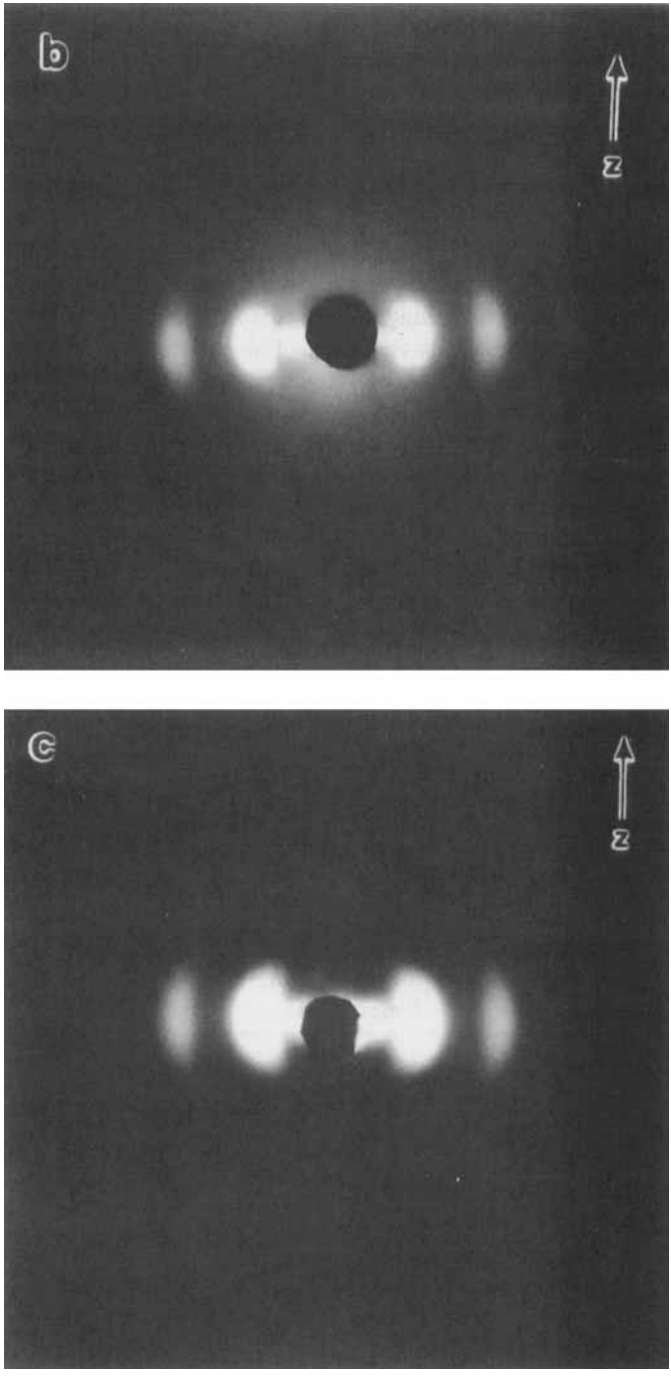

Fig 7(b) and 7(c)

of scattering, but more noteworthy is the strong azimuthal dependence which is due to the orientation of the morphological structure, i.e., "slitlike" scattering. Assuming that the scattering represents four orders, the Bragg spacing calculated from the edge-shot patterns provides the same result as that from the pattern in Fig. 7(a) and again is in good direct agreement with the "side-view" TEM experiments.

At this point the SAXS results, in conjunction with the side-view TEM micrographs, strongly support the presence of a lamellar texture. There is, however, some question concerning this proposed structure if the TEM micrographs of the perpendicular view to the film surface is taken into account, i.e., a lamellar structure was not directly seen, but rather the micrograph suggests a structure that could arise from rodlike units being viewed end on. Indeed, the salt-and-pepper pattern observed in this direction was believed real in view of the analysis of the microscopy procedures utilized, i.e., the defocusing analysis. Hence, there is some question whether the structure is truly a lamellar texture as based on the perceived four orders of scattering by the SAXS analysis, or whether there may be more of a rodlike packing which would not be expected to lead to the same equivalent SAXS interpretation of the four scattering peaks having a Bragg spacing ratio of approximately 1:2:3:4. We therefore considered further the system in view of possible line-broadening effects that occur in the SAXS data (Figs. 3 and 7) and what the general spacing ratios are as determined from several samples. From both the desmeared Kratky data as well as several patterns collected with the Warhus camera we provide Table 3, which presents the average d spacing along with the associated error range based on our analysis.

TABLE 2. Interdomain Spacing of Ionene Polymers

Sample	d Spacing, nm,[a] (smeared)	RMS,[b] nm
IB-NS-18	7.0	3.7
IB-NS-26	7.8	4.7
IB-NS-34	8.0	5.4
IB-NS-66	9.3	7.5

[a] $s = (2/\lambda) \sin \theta$.

[b] RMS is the estimated root-mean-square end-to-end distance calculated by using a Gaussian approximation for the PTMO segment.

TABLE 3. d Spacing of IB-NS-18 Ionene from Warhus Camera Results

d Spacing, nm	d_1	d_2	d_3	d_4
Average d	6.51	3.31	2.21	1.66
Relative spacing	1	1.97	2.95	3.92
Error range $\pm 2\sigma$[a]	6.51 ± 0.6	3.31 ± 0.18	2.21 ± 0.1	1.66
Relative spacing	0.9-1.1	1.69-2.27	2.56-3.37	3.56-4.28
Measured d spacing	5.24-6.99	3.15-3.50	2.15-2.31	1.66
Relative spacing		1.5-2.22	2.27-2.74	3.15-4.21

[a]σ is the standard deviation of the d spacing.

Note in Table 3 that the ratios of the relative Bragg spacings are in a range of 0.9-1.1:1.69-2.27:2.56-3.7:3.56-4.28. While these data might again strongly support the general lamellar texture in that the four spacings do occur in a range of ratios 1:2:3:4, there is some question whether this interpretation is correct. For example for oriented cylindrical particles packed in a hexagonally close-packed array, the same spacing ratios are determined to be 1:1.73; 2:2.65; 3:3.5; 3.6:4. Since we can only observe four scattering peaks that are somewhat broadened, it is possible that our system might well also have the character of a cylindrically hexagonally packed array if the long-range order is limited in the system, thereby leading to line broadening and causing some of the expected peaks from a cylindrically packed array to be overlapped as has been observed and discussed for block copolymer systems by Hashimoto [35]. Hence, there is the possibility that, having only four broad scattering peaks to work with, we cannot conclude firmly that it is either a lamellar or a hexagonally packed cylindrical domain texture although our earlier discussion strongly suggested a lamellar morphology based principally on the SAXS results in the side-view TEM micrographs.

Extending our discussion of the possibility for a hexagonally packed system of rodlike domains, we have also considered estimating the volume fraction of the ionene domains that would occur for this morphological structure as for a continuous lamellar morphology. Using an interdomain spacing of 6.5 nm as based on the SAXS data and assuming complete phase separation, i.e., sharp interfaces, a rough calculation of these volume fractions can be made. To carry out this calculation, an estimate of the domain width is needed, and an upper and lower bound of 1.5 and 1.1 nm has been utilized in view

of chemical bond lengths as well as including the large bromide counterions. While, indeed, the ionene unit is not disk shaped, we have ignored this in the calculation and considered its length as the diameter for the rod calculation as well as the width dimension for the lamellar structure. If we use the upper and lower bounds for these diameters or widths, our calculations indicate that the minimum ionene domain volume fraction would be 5.3% for the hexagonal rod packed system versus 23.1 vol% for the lamellar structure with the 1.5-nm dimension. In the case of the 1.1-nm dimension, the minimum ionene domain volume required would be 2.8 vol% for the hexagonally packed rod structure and 19.9 vol% for the lamellar texture. Further details of calculations are given in the Appendix.

Our estimates of the ionene volume content strongly suggest that it is unlikely to form a continuous lamellar domain structure in the IB-NS-18 ionene sample. In fact, for this material the ionene segment volume is estimated to be 6.4 vol% based on chemical composition and estimated densities of the relative components. This number barely satisifies the minimum required hard segment volume for the hexagonally packed structure but clearly is far below that expected for a lamellar texture. Hence, consideration of the ionene volume estimations above, the possibility of line broadening influencing the SAXS results, and finally both the normal and perpendicular views of our material by TEM, we tentatively propose that the morphological structure may well be best described by a system of hexagonally packed rods with some degree of irregularity in contrast to a lamellar texture. The proposed domain structure and arrangement of the ionene moieties of IB-NS-18 is shown in Fig. 8. In this model the ionene segments form rodlike domains which orient perpendicular to the surface of the solution cast film. Due to the wavy nature of these rodlike domains, their volume fraction shown in the TEM micrograph viewed normal to the surface would indeed be greater than expected in line with the observation. This wavy nature also reduces the long-range order of the structure which leads to some line broadening effect on the SAXS results.

CONCLUSIONS

We have illustrated for the first time a direct observation of the microphase separation induced in ionene polymers by transmission electron microscopy. The microstructure observed by TEM is quite well in line with the interpretation of the SAXS results. However, in view of potential line broadening features of the SAXS data, we are unable to unequivocally specify that the morphological texture is either lamellar or that formed by a hexagonal array of

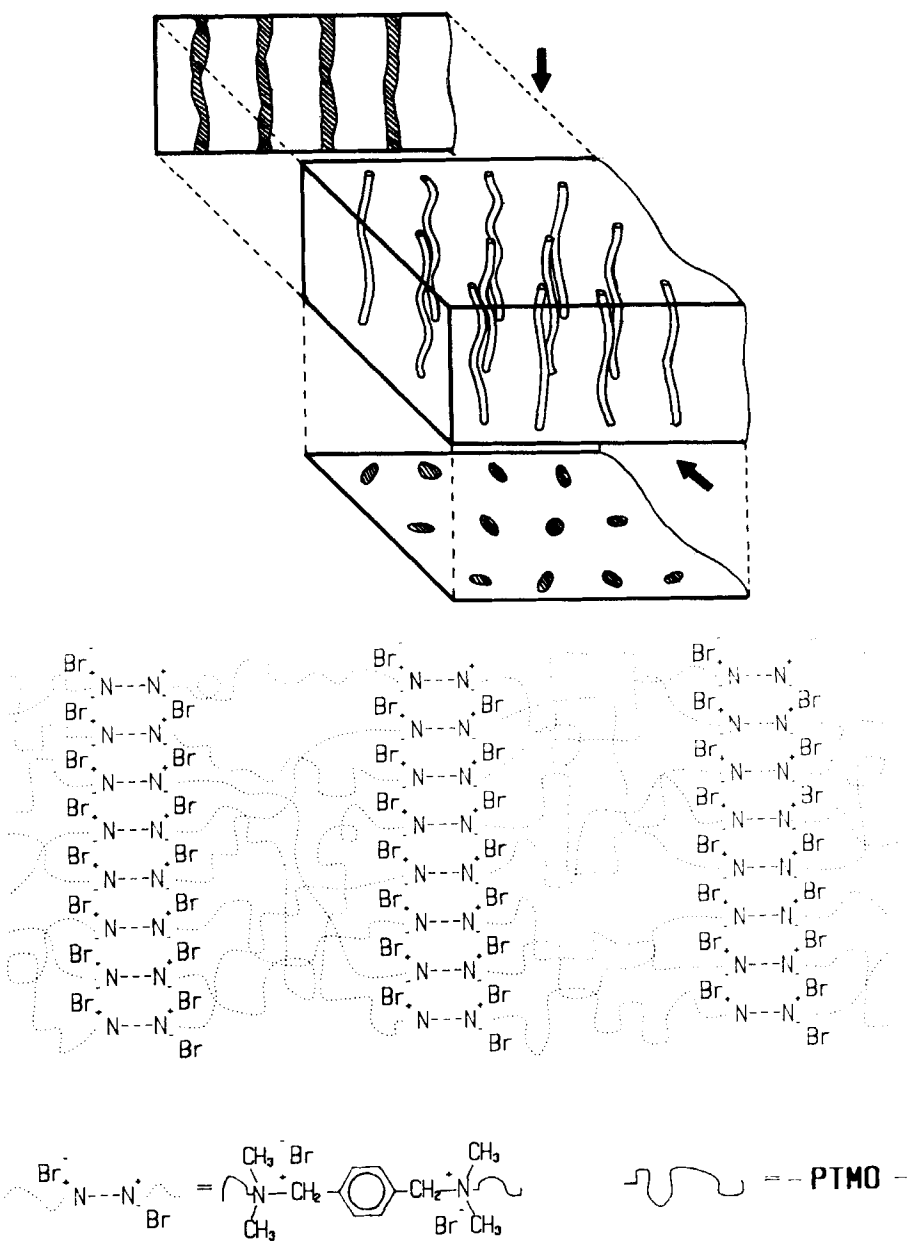

FIG. 8. Proposed tentative domain structure of IB-NS-18 ionene polymer. (a) Domain structure of IB-NS-18 ionene. (b) Simplified arrangement of ionene moieties of IB-NS-18 ionene.

cylindrical ionene domains. We do, however, favor the latter model for the reasons discussed.

We finally point out that the morphological texture observed in the ionene materials can be influenced by the solution-casting procedure although this has not been discussed in great detail in this paper. Specifically, as the PTMO segment length increases, which reduces the volume fraction of the ionene component, the distinct morphological texture can no longer be directly observed by TEM, and the azimuthal dependence of the SAXS intensities for the side-view profiles disappears systematically. This suggests that, as the volume fraction of the ionene component decreases to very low percentages, this long-range order is no longer maintained but rather leads to a more random distribution of the ionic domains.

APPENDIX: ESTIMATION OF THE VOLUME OCCUPIED BY THE IONENE DOMAINS

The volume fraction of ionene domains in IB-NS-18 has been estimated by assuming continuous hexagonal packed rodlike or lamellar domains. In these estimations, the length of the domains is assumed to be the same as the height of the unit volume. The other parameters used are defined as follows:

d = interdomain spacing
D = domain size (diameter of domain or lamellar thickness), which is assumed to be the length of an ionene unit
L^2 = unit area, which is defined as $L^2 = (10d)^2$
V = unit volume, which equals L^2H
H = height of unit volume
V_h = volume of an ionene domain
f_h = volume fraction of ionene domains
n = number of rods or lamellae per unit volume (n = 126 for hexagonal packed rodlike domains in a unit area; n = 10 for lamellar domains in a unit area)

For hexagonal packed domains:

$$f_h = \frac{V_h n}{V} = \frac{\pi/4 D^2 nH}{L^2 H}.$$

For lamellar domains:

$$f_h = \frac{V_h n}{V} = \frac{DLHn}{L^2 H}.$$

The calculation results are listed in the following table:

	Ionene domain, vol%	
Ionene domain size, nm	Hexagonal	Lamellar
1.1	2.8	16.9
1.5	5.3	23.1

ACKNOWLEDGMENTS

The Virginia Polytechnic Institute and State University authors would like to express their appreciation to the American Chemical Society (PRF Grant #15441-8C7) and the Army Research Office for support of this work.

REFERENCES

[1] D. Graiver, M. Litt, and E. Baer, *J. Polym. Sci., Polym. Chem. Ed., 17,* 3573 (1979).
[2] A. Eisenberg and M. King, *Ion Containing Polymers; Physical Properties and Structure* (Polymer Physics 2, R. S. Stein, ed.), Academic, New York, 1977.
[3] D. J. Yarusso and S. L. Cooper, *Macromolecules, 16,* 1871 (1983).
[4] A. Eisenberg, *Ibid., 3,* 147 (1970).
[5] C. G. Bazuim and A. Eisenberg, *Ind. Eng. Chem., Prod. Res. Dev., 20,* 271 (1981).
[6] A. F. Galambos, W. B. Stockton, J. K. Koberstein, A. Sen, R. A. Weiss, and T. P. Russell, *Macromolecules, 20,* 3091 (1987).
[7] E. J. Roche, PhD Thesis, University of Massachusetts, 1978.
[8] W. J. MacKnight, W. P. Taggart, and D. J. Stein, *J. Polym. Sci., Polym. Symp., 45,* 113 (1974).

[9] C. L. Marx, J. A. Koutsky, and S. L. Cooper, *J. Polym. Sci., Part B, 9,* 169 (1971).
[10] P. J. Phillips, *J. Polym. Sci., Polym. Lett. Ed., 10,* 443 (1972).
[11] D. L. Handlin, W. J. MacKnight, and E. L. Thomas, *Macromolecules, 14,* 795 (1981).
[12] M. Pineri and A. Eisenberg (eds.), *Structure and Properties of Ionomers,* NATO ASI Series, Reidel, Dordrecht, 1987, pp. 453-456.
[13] A. Rembaum, W. Baumgatner, and A. Eisenberg, *J. Polym. Sci., B, 6,* 159 (1968).
[14] T. Hashimoto, M. Shibayama, M. Fujimura, and H. Kawai, *Mem. Fac. Eng., Kyoto Univ., 43*(2), 184 (1981).
[15] C. M. Leir and J. E. Stark, *J. Appl. Polym. Sci.,* Submitted.
[16] T. P. Klun, L. A. Wendling, J. W. C. van Bogart, and A. F. Robbins, *J. Polym. Sci., Polym. Chem. Ed., 25,* 87 (1987).
[17] D. Feng, L. N. Venkateshwaran, and G. L. Wilkes, *J. Appl. Polym. Sci.,* Submitted.
[18] J. W. Cowley, *Diffraction Physics,* North-Holland, Amsterdam, 1975.
[19] H. P. Erickson, *Adv. Opt. Electron Microsc., 5,* 163 (1973).
[20] B. L. Misell, in *Practical Methods in Electron Microscopy,* Vol. 7 (A. M. Glauert, ed.), North-Holland, New York, 1978.
[21] E. L. Thomas and E. J. Roche, *Polymer, 20,* 1413 (1979).
[22] E. J. Roche and E. L. Thomas, *Ibid., 22,* 333 (1981).
[23] D. L. Handlin, PhD Thesis, University of Massachusetts, 1986.
[24] E. L. Thomas, in *Structure of Crystalline Polymers* (H. I. Hall, ed.), Elsevier, New York, 1984, pp. 79-124.
[25] R. E. Burge and G. H. Smith, *Proc. Phys. Soc., 79,* 673 (1962).
[26] H. P. Erikson and A. Klug, *Philos. Trans. R. Soc. London, B261,* 105 (1971).
[27] J. A. Ibers, D. H. Templeton, B. K. Vainshtein, G. E. Bacon, and K. Lonsdale, in *International Tables for X-Ray Crystallography,* Vol. III, 1962, p. 201.
[28] M. R. Tant, PhD Thesis, Virginia Polytechnic Institute and State University, 1986.
[29] G. Broze, T. Jerome, Ph. Teyssié, and B. Gallo, *J. Polym. Sci., Polym. Lett. Ed., 19,* 415 (1981).
[30] L. N. Venkateshwaran, Personal Communication.
[31] A. W. Agar, R. H. Alderson, and D. Chescoe, *Principles and Practice of Electron Microscope Operation,* North-Holland, Amsterdam, 1974.
[32] E. L. Thomas, in *Encyclopedia of Polymer Science and Engineering,* 2nd ed., Wiley, New York, 1987, pp. 644-687.

[33] D. Tyagi, J. E. McGrath, and G. L. Wilkes, *Polym. Eng. Sci., 26,* 1371 (1986).
[34] T. Hashimoto, K. Nagatoshi, A. Todo, H. Hasegawa, and H. Kawai, *Macromolecules, 7,* 364 (1974).
[35] T. Hashimoto, Y. Tsukahara, K. Tachi, and H. Kawai, *Ibid., 16,* 648 (1983).

Received January 15, 1989